Available online at www.sciencedirect.com
ScienceDirect
Trans. Nonferrous Met. Soc. China 24(2014) 3142−3151
Transactions of Nonferrous Metals Society of China
www.tnmsc.cn

Microstructure and magnetic properties of anisotropic Nd−Fe−B magnets prepared by spark plasma sintering and hot deformation

Xiao-qiang LI, Li LI, Ke HU, Zhi-cheng CHEN, Sheng-guan QU, Chao YANG

National Engineering Research Center of Near-net-shape Forming Technology for Metallic Materials, South China University of Technology, Guangzhou 510640, China

Received 12 October 2013; accepted 21 March 2014

Abstract: Bulk anisotropic Nd−Fe−B magnets were prepared from hydrogen−disproportionation−desorption−recombination (HDDR) powders via spark plasma sintering (SPS) and subsequent hot deformation. The influence of sintering temperature on the structure and magnetic properties of the spark plasma sintered Nd−Fe−B magnets were studied. The remanence B_r, intrinsic coercivity H_{cj}, and the maximum energy product $(BH)_{max}$, of sintered Nd−Fe−B magnets first increase and then decrease with the increase of sintering temperature, T_{SPS}, from 650 °C to 900 °C. The optimal magnetic properties can be obtained when T_{SPS} is 800 °C. The Nd−Fe−B magnet sinter treated at 800 °C was subjected to further hot deformation. Compared with the starting HDDR powders or the SPS treated magnets, the hot-deformed magnets present more obvious anisotropy and possess much better magnetic properties due to the good *c*-axis texture formed in the deformation process. The anisotropic magnet deformed at 800 °C with 50% compression ratio has a microstructure consisting of well aligned and platelet-shaped $Nd_2Fe_{14}B$ grains without abnormal grain growth and exhibits excellent magnetic properties parallel to the pressing axis.

Key words: Nd−Fe−B magnet; hydrogen−disproportionation−desorption−recombination (HDDR); spark plasma sintering; hot deformation; magnetic property

1 Introduction

Nd−Fe−B-based sintered magnets exhibit outstanding magnetic performance among various permanent magnets of today, and they have been used in a wide variety of applications, such as traction motor for hybrid and pure electric vehicles, speakers of mobile phone and magnetic resonance imaging (MRI) [1,2]. There are three different routes for preparing Nd−Fe−B magnets, including bonding, sintering and hot deformation (HD). The major limitation needs to be addressed for widespread use of bonded magnets applications: the low magnetic properties. Compared with sintering process, the HD process is commonly used to achieve good *c*-axis texture and magnetic anisotropy. Hot deformed Nd−Fe−B magnets have attracted much attention due to their good magnetic performance together with desirable thermal stability, corrosion resistance and fracture toughness [3,4]. However, their preparation technique is still a major concern, since their magnetic properties deteriorate dramatically due to excessive grain growth during the densification and deformation process by conventional methods [5,6].

Hydrogen − disproportionation − desorption − recombination (HDDR) process has been widely established to produce Nd−Fe−B powders which are composed of very fine $Nd_2Fe_{14}B$ phase grains of nearly single domain size (~240 nm) [7]. Although anisotropic HDDR powders are now used to produce anisotropic bonded magnets only [8], they can be excellent raw materials for anisotropic HD treated magnets as well from their very fine grain size [9]. However, there are two major problems needed to be resolved for the widespread application of HDDR-processed Nd−Fe−B magnets. One is that the relatively low coercivity H_{cj} because of insufficient magnetic isolation among grains should be improved [10]. The other problem is how to enhance the relatively low B_r due to the poor crystallographic texture. A magnetic and crystallographic texture can be induced by hot deformation, resulting in an axial alignment of $Nd_2Fe_{14}B$ grains with their easily

Foundation item: Project (NCET-10-0364) supported by the Program for New Century Excellent Talents in University, China; Project (2012ZG0006) supported by the Fundamental Research Funds for the Central Universities, China; Project (51174095) supported the National Natural Science Foundation of China

Corresponding author: Ke HU; Tel/Fax: +86-20-87112111; E-mail: kehuscut@gmail.com

DOI: 10.1016/S1003-6326(14)63453-1

magnetized *c*-axis parallel to the compression direction [11−13]. Due to the high sintering temperature, the main disadvantages of the Nd−Fe−B magnets fabricated by conventional sintering methods are the existence of large-sized grains, non-magnetic phase and non-uniform microstructure, which lead to low magnetization, poor corrosion resistance and weak temperature stability [14,15]. Spark plasma sintering (SPS) is an unique technique that can restrain grain growth effectively and allow the consolidation of ultrafine grained powders [16]. By SPS technique, fully dense isotropic and anisotropic nanostructured Nd−Fe−B permanent magnets have been prepared successfully [6,9,17]. In the present work, isotropic and anisotropic Nd−Fe−B magnets were prepared from HDDR powders by SPS and by SPS+HD, respectively. The major aim is to explore the effects of SPS temperature, T_{SPS}, hot deformation temperature, T_{HD} and compression ratio on the microstructure and magnetic properties of the magnets.

2 Experimental

The starting materials were commercial HDDR powders (AHP-II, Jilin Huisheng Strong Magnet Co. Ltd., China). The composition of the HDDR powders was measured by an inductive coupled plasma emission spectrometer (ICP, ULTIMA2, France). Every time 25 g powders were poured into a 20.4 mm-inner-diameter graphite die for SPS on the SPS−825 sintering machine (Dr. Sinter825, Sumitomo Coal Mining Co. Ltd., Japan). The SPS conditions were sintering temperature T_{SPS} of 650−900 °C, holding time t_{SPS} of 20 min, sintering pressure p_{SPS} of 50 MPa and residual cell pressure less than 8 Pa. The sample sintered at 800 °C was subsequently hot deformed on the SPS−825 sintering machine by SPS technique. The hot deformation was carried out in an open WC die at various temperatures ranging from 750 to 900 °C with true strain rate of 0.001 s^{-1} to obtain a height reduction of 41%−69%. A cylindrical specimen with sizes of *d*2 mm×2 mm was cut from the center of the HDed sample for further analysis of microstructure and property. Magnetic properties of the HDDR powders, SPS treated magnets and HD treated magnets at room temperature were measured by a physical property measurement system equipped with a 8 T vibrating sample magnetometer (PPMS−9, Quantum Design, USA). The crystal structure of the magnets was investigated with an X-ray diffractometer using Cu K_α radiation(X-pert, Philip, Holland). The density (ρ) was determined by Archimedes method. The fractured surfaces of the magnets were observed by scanning electron microscopy (Nano430, FEI Co., USA).

3 Result and discussion

3.1 Effect of T_{SPS} on microstructure and phase structure of SPS treated Nd−Fe−B magnets

Figure 1(a) shows the morphology of the starting HDDR powders. The powders have non-uniform size and irregular shape. The composition, density, size and magnetic properties of the HDDR powders are shown in Table 1 (composition and magnetic property of the powders are obtained by ICP and PPMS−9, respectively; particle size and density of the powders are provided by supplier). The powders exhibit magnetic properties (without considering the demagnetizing factor): B_r of 0.74 T, H_{cj} of 974 kA/m, and $(BH)_{max}$ of 79 kJ/m^3. The low coercivity originates from the Nd-lean composition. A back scattered electron image for the typical structure of SPS treated Nd−Fe−B magnets is shown in Fig. 1(b). Table 2 shows the EDS analysis results of the phase in Fig. 1(b). In the SPSed Nd−Fe−B magnet, discontinuous Nd-rich phase decorates along the powder surfaces.

Figure 2 shows the XRD patterns obtained from the surface perpendicular to the pressing axis of the Nd−Fe−B magnets sintered at various temperatures (p_{SPS}=50 MPa and t_{SPS}=20 min). All peaks in all patterns

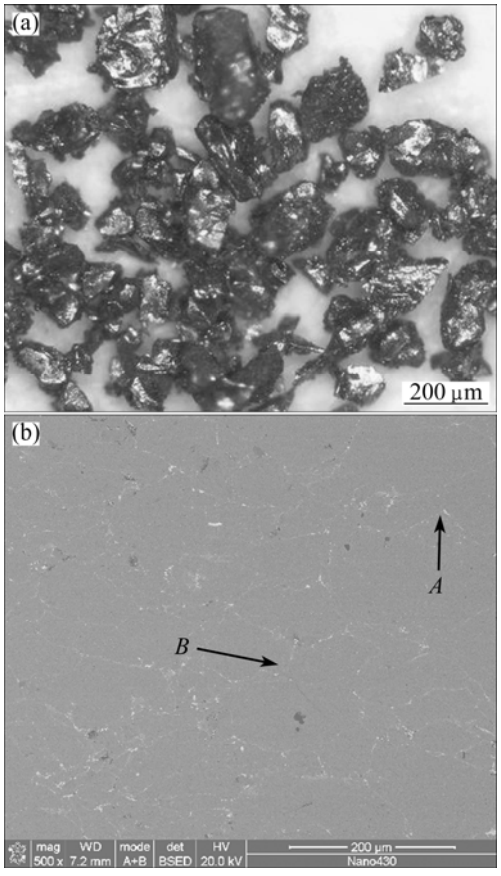

Fig. 1 Optical image for starting HDDR powders (a) and back scattered electron image for typical structure of SPS treated Nd−Fe−B magnet (b)

Table 1 Composition, density, size and magnetic properties of HDDR powders

Composition/%	Density/(g·cm^{-3})	Powder size/μm	B_r/T	H_{cj}/(kA·m^{-1})	$(BH)_{max}$/(kJ·m^{-3})
$Nd_{26.64}Fe_{69.95}Al_{0.38}B_1$	7.64	50−200	0.74	973.93	79.35

Table 2 EDS analysis of phase in Fig. 1(b)

Point	x(Nd)/%	x(Fe)/%	x(Nd):x(Fe)	Phase
A	19.34	52.17	2 : 5	Nd-rich
B	10.33	72.85	2 : 14	$Nd_2Fe_{14}B$

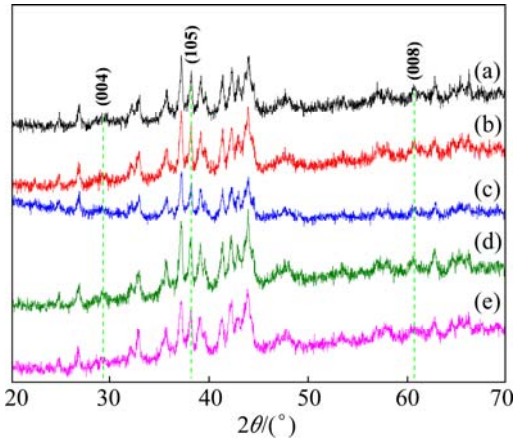

Fig. 2 XRD patterns obtained from surface perpendicular to pressing direction of Nd−Fe−B magnets sintered at different temperatures with p_{SPS}=50 MPa and t_{SPS}=20 min: (a) 650 °C; (b) 700 °C; (c) 750 °C; (d) 800 °C; (e) 900 °C

are attributed to the tetragonal hard magnetic $Nd_2Fe_{14}B$ phase (the serial number of the standard PDF of $Nd_2Fe_{14}B$ is 39−0473), indicating no significant change in phase structure. For the sample sintered at 800 °C, the (00*l*) peaks and the peaks for the planes with direction close to (00*l*), such as (004), (008) and (105) peaks, have enhanced intensity. This indicates a slight *c*-axis crystallographic alignment of the magnet, although the alignment is not as strong as in the HD treated Nd−Fe−B magnets [15].

The microstructures of the magnets SPSed at 650−900 °C for 20 min with p_{SPS}=50 MPa are shown in Fig. 3. With increasing the T_{SPS} in the range of 650−900 °C, the number and size of the pores in the sintered magnets gradually reduce and few pores can be observed in the magnets sintered at 800 °C. This indicates that the SPSed magnets are nearly fully dense when T_{SPS} comes up to 800 °C, whereas conventional liquid phase sintering generally requires the temperature above 1100 °C for 1−2 h to obtain the density [18]. A liquid Nd-rich grain-boundary phase is present at around 670 °C [19] and its volume fraction and fluidity increase with the increase of T_{SPS} [20]. When T_{SPS} reaches 800 °C or above, the volume fraction of Nd-rich liquid grain-boundary phase with good fluidity is large enough to fill the pores. Otherwise, the remaining pores will lead to a low density and bad magnetic properties. The insets of Figs. 3(c), (d) and (e) show the $Nd_2Fe_{14}B$ grain size and shape in Nd−Fe−B magnets SPS treated at 750, 800 and 900 °C, respectively. The equiaxed $Nd_2Fe_{14}B$ grains in Nd−Fe−B magnets SPS treated at 750 °C are quite different from aligned platelet grains sintered at 800 °C as reported by LEONOWICZ et al [21]. Compared with the magnet sintered at 800 °C, the abnormal grain growth is obvious in the magnet sintered at 900 °C since the higher temperature provides extra energy [17]. It is believed that this microstructure characteristic has an important effect on the magnetic properties.

3.2 Effect of T_{SPS} on magnetic properties

The magnetic hysteresis curves (along the pressing axis) of the Nd−Fe−B magnets SPS treated at various temperatures are shown in Fig. 4. The hysteresis loops with nice squareness were obtained for all the SPS treated Nd−Fe−B magnets, indicating good hard magnetic properties [17]. Table 3 shows the magnetic properties (parallel (//) and perpendicular (⊥) to the pressing axis) of the Nd−Fe−B magnets SPS treated at various temperatures. The sintering temperature plays an important role in the density and magnetic properties of the Nd−Fe−B magnets. With increasing the sintering temperature in the range of 650−900 °C, the remanence B_r, coercivity H_{cj} and maximum energy product $(BH)_{max}$ all increase first and then decrease. The optimal magnetic properties of $B_r^{//}$=0.78 T, $H_{cj}^{//}$=577 kA/m, $(BH)_{max}^{//}$= 78 kJ/m^3 are obtained in the samples SPS treated at 800 °C and the sintered density reaches 99% of the theoretical value. The increase in T_{SPS} causes a gradual augment in sintered density, which is consistent with the changing trend of pores in the magnets (see Fig. 3). The $B_r^{//}$ is 21% higher than the $B_r^{\perp}$ for the magnets sintered at 800 °C, indicating magnetic anisotropy. This agrees well with the above analysis of XRD patterns (Fig. 2) and SEM images of the fractured surfaces (Fig. 3(d)). The magnet sintered at 900 °C is also anisotropic with its $B_r^{//}$ of 25% higher than $B_r^{\perp}$. However, the magnet sintered at 750 °C is isotropic and its $B_r^{//}$ and $B_r^{\perp}$ approximate. The anisotropic microstructure leads to the magnetic anisotropy and better magnetic properties, e.g., for the samples SPS treated at 800 °C. Although the magnet SPS treated at 900 °C is also anisotropic, it has poor magnetic properties because the abnormal grain growth is harmful to B_r and H_{cj}. While T_{SPS} reaches 800 °C or above, the $Nd_2Fe_{14}B$ grains are surrounded by large volume

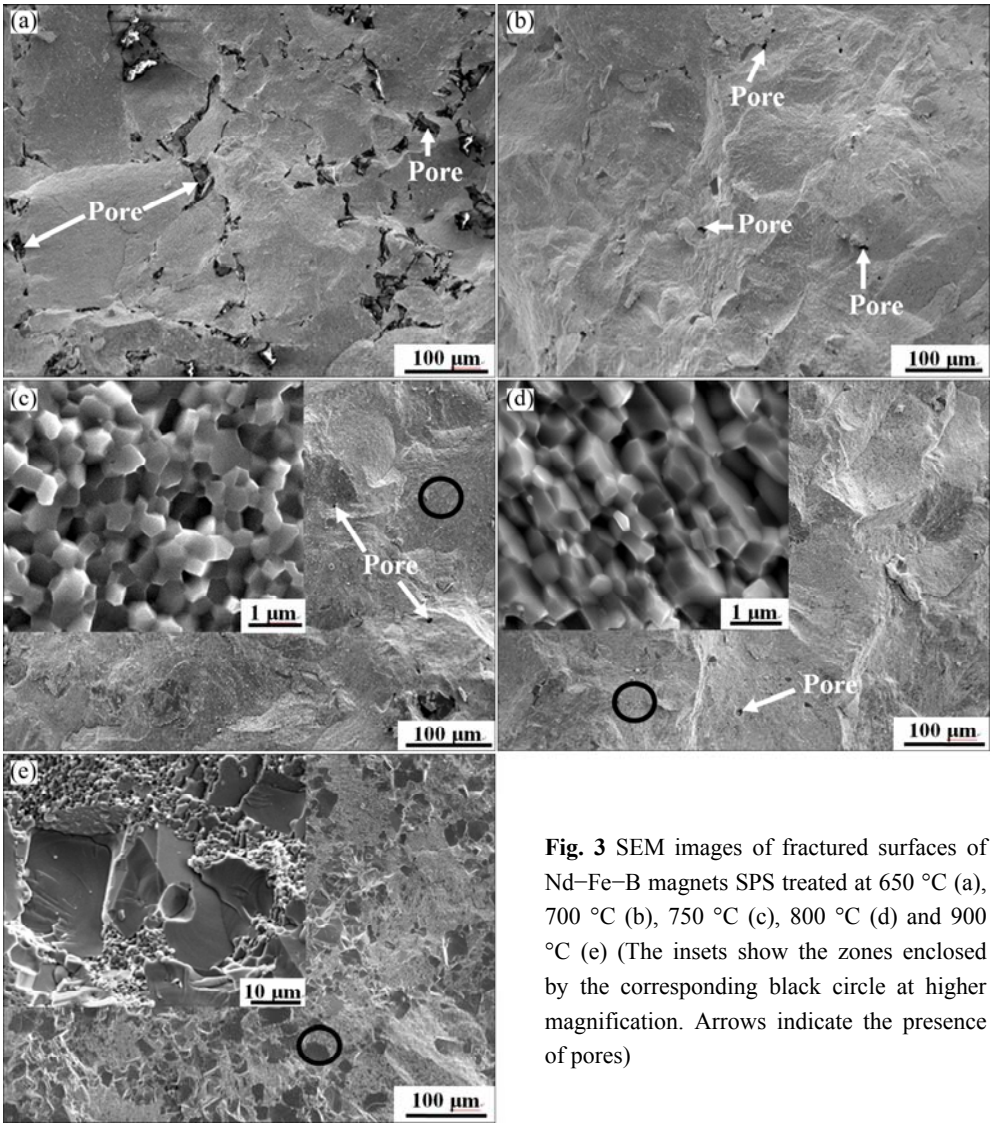

Fig. 3 SEM images of fractured surfaces of Nd−Fe−B magnets SPS treated at 650 °C (a), 700 °C (b), 750 °C (c), 800 °C (d) and 900 °C (e) (The insets show the zones enclosed by the corresponding black circle at higher magnification. Arrows indicate the presence of pores)

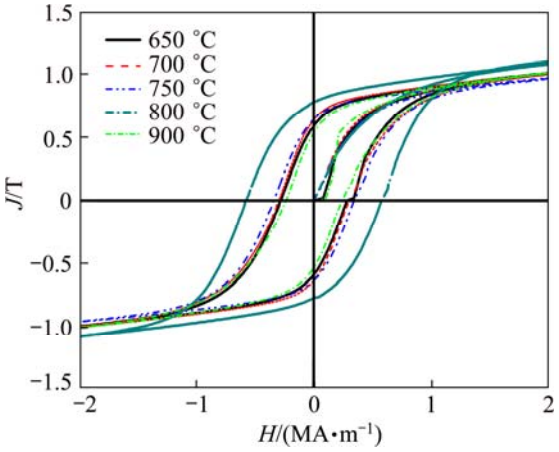

Fig. 4 Magnetic hysteresis curves (along pressing axis) of Nd−Fe−B magnets SPS treated at different temperatures (p_{SPS}=50 MPa, t_{SPS}=20 min)

fractions of liquid Nd-rich grain boundary phase and the $Nd_2Fe_{14}B$ grains will preferentially grow perpendicularly to the pressing direction under the combination of the sintering pressure, electric current and heat. However, the preferential growth of $Nd_2Fe_{14}B$ grains is not very obvious due to the restriction from the graphite die. On the other hand, the isotropic performance of the magnets sintered below 800 °C is due to the lack of the preferential growth of $Nd_2Fe_{14}B$ grains resulting from the small volume fraction of liquid Nd-rich grain boundary phase during sintering.

Table 3 Density and magnetic properties of SPS treated magnet at different temperatures (P_{SPS}=50 MPa, t_{SPS}=20 min)

T_{SPS}/ °C	ρ/ (g·cm^{-3})	$B_r^{//}$/ T	$B_r^{\perp}$/ T	$(B_r^{//}-B_r^{\perp})/B_r^{//}$	$H_{cj}^{//}$/ (kA·m^{-1})	$(BH)_{max}^{//}$/ (kJ·m^{-3})
650	7.09	0.58	−	−	282	30
700	7.34	0.63	−	−	297	36
750	7.56	0.64	0.58	9	340	41
800	7.58	0.78	0.62	21	576	78
900	7.59	0.53	0.40	25	238	23

3.3 Effect of hot deformation process on microstructure and phase constitution

Figure 5 shows the XRD patterns obtained from the surface perpendicular to the pressing direction of the magnet SPS treated at 800 °C and the magnets further HD treated under the various deformation conditions. For the SPS treated and HD treated Nd−Fe−B magnets, all the diffraction peaks are attributed to the tetragonal hard magnetic $Nd_2Fe_{14}B$ phase. In contrast with the SPS treated magnet, the (00*l*) peaks and the peaks with direction close to (00*l*) of the HD treated magnets, such as (004), (105), (006) and (008) peaks, have obviously enhanced intensities, indicating a stronger *c*-axis crystallographic alignment. As shown in Figs. 5(b) and (c), the intensities of the (004), (105), (006) and (008) peaks also increase with the deformation temperature rising from 750 °C to 800 °C. Moreover, with increasing the compression ratio from 41% to 60%, the relative intensities of the (004), (105), (006) and (008) diffraction peaks become stronger gradually (see Figs. 5(c), (d), and (e)), which means the increase of *c*-axis crystallographic alignment. The degree of texture $[(B_r^{//}-B_r^{\perp})/B_r^{//}]$ can be used to characterize the mean alignment of *c*-axis texture of $Nd_2Fe_{14}B$ grains along the pressing axis. The degree of texture increases with increasing the compression ratio and deformation temperature as listed in Table 4. The variation is consistent with the XRD results.

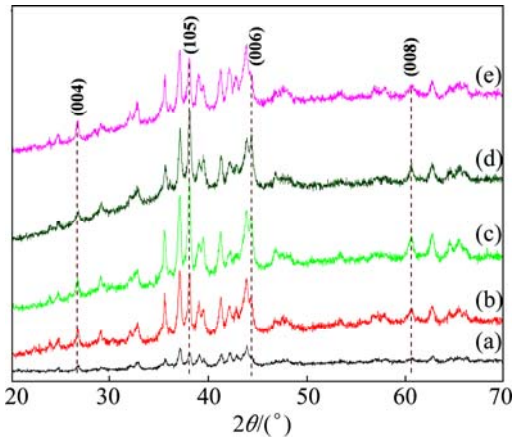

Fig. 5 XRD patterns (obtained from surface perpendicular to pressing direction) for magnet SPS treated at 800 °C (a) and magnets further HD treated at 750 °C, 60% (b), 800 °C, 60% (c), 800 °C, 50% (d) and 800 °C, 41% (e)

Figure 6 shows the microstructures of the HD treated magnets. With the deformation temperature increasing from 750 °C to 900 °C, the crystallographic alignment of $Nd_2Fe_{14}B$ grains along the pressing axis is enhanced gradually, indicating a gradually strong magnetic anisotropy. This is also consistent with the XRD results. The microstructure of the magnets HD treated at 750 °C with a compression ratio of 60% consists of two different types of $Nd_2Fe_{14}B$ grains: a large volume fraction of $Nd_2Fe_{14}B$ grains with (001) crystal plane parallel to the pressing axis (see Fig. 6(a)) and ellipsoidal-shaped ones (see Fig. 6(b)).

The deformation mechanism of Nd−Fe−B magnets is widely believed to be a stress-induced preferential grain growth via dissolution and precipitation [22]. Additionally, the liquid Nd-rich grain boundary phase acts as a lubricant between $Nd_2Fe_{14}B$ grains and a diffusion path for mass transport, which is necessary for the formation of good texture during the hot deformation [22]. The origin of the Nd-rich phase at the grain boundary has been explained due to the diffusion of Nd from an excess of Nd in the hard magnetic regions after hydrogen desorption [23]. The Nd-rich grain boundary phase exists as a liquid when the hot deformation temperature is 750 °C (just above 670 °C), and it may have low fluidity. Meanwhile, the dissolution of the unfavorable $Nd_2Fe_{14}B$ grains (their *c*-axes are out of the pressing axis) into the liquid grain boundary phase may not be affluent because of the relatively low temperatures. Thus, little material can be dissolved from the unfavorable $Nd_2Fe_{14}B$ grains and it is hardly transported

Table 4 Magnetic properties and degree of texture of SPS treated and HD treated magnets

Processing	B_r/T		H_{cj}/(kA·m^{-1})		$(BH)_{max}$/(kJ·m^{-3})		$(B_r^{//}-B_r^{\perp})/B_r^{//}$
	//	⊥	//	⊥	//	⊥	
800 °C, SPS	0.78	0.62	577	638	78	54	0.2051
750 °C, 60%	1.15	0.32	228	419	139	13	0.7217
800 °C, 60%	1.19	0.33	285	495	143	15	0.7227
850 °C, 60%	1.2	0.31	221	458	140	13	0.7417
900 °C, 60%	1.21	0.29	229	398	141	11	0.7603
800 °C, 41%	1.06	0.45	366	589	139	28	0.5755
800 °C, 47%	1.08	0.45	398	569	141	28	0.5833
800 °C, 50%	1.16	0.38	449	636	178	21	0.6724
800 °C, 69%	1.22	0.23	181	331	121	7	0.8115

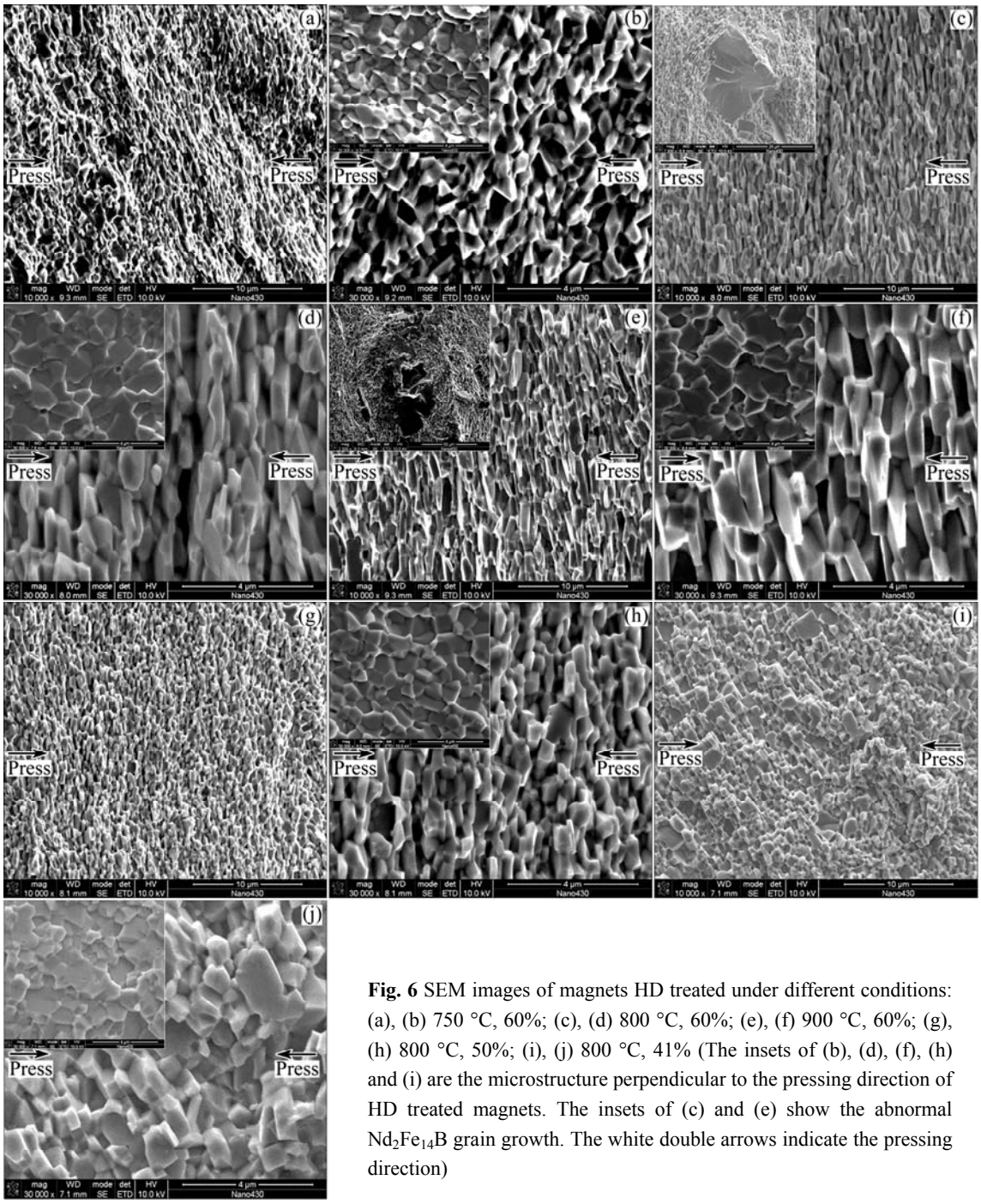

Fig. 6 SEM images of magnets HD treated under different conditions: (a), (b) 750 °C, 60%; (c), (d) 800 °C, 60%; (e), (f) 900 °C, 60%; (g), (h) 800 °C, 50%; (i), (j) 800 °C, 41% (The insets of (b), (d), (f), (h) and (i) are the microstructure perpendicular to the pressing direction of HD treated magnets. The insets of (c) and (e) show the abnormal $Nd_2Fe_{14}B$ grain growth. The white double arrows indicate the pressing direction)

towards the favorable $Nd_2Fe_{14}B$ grains (their *c*-axes are parallel to the pressing axis) through the liquid grain boundary phase, which leads to poor texture [11]. Higher hot deformation temperature, 800 °C, with compression ratio of 60%, produces much better alignment of $Nd_2Fe_{14}B$ grains, which is evidenced from the corresponding microstructure (Figs. 6(c), (d)) and XRD results (Fig. 5). From Fig. 6(d), the platelet-shaped $Nd_2Fe_{14}B$ grains have sizes of 470 nm (*h*)×1320 nm (*w*) nm and their (001) planes are aligned parallel to the pressing axis, where *w* and *h* respectively represent the mean grain size perpendicular or parallel to the pressing direction. The inset of Fig. 6(c) shows the abnormal $Nd_2Fe_{14}B$ grain growth which will deteriorate the magnetic properties. The abnormal grain growth arises from longer time at a high temperature to finish a greater compression ratio such as 60%. The hot deformation at 900 °C with compression ratio of 60% results in more serious abnormal grain growth (see Figs. 6(e) and (f))), because of higher deformation temperature. The mean size of $Nd_2Fe_{14}B$ grains also goes up to 570 nm (*h*), 1576 nm (*w*).

At a certain deformation temperature such as 800 °C, the *c*-axis texture becomes stronger with the increase of compression ratio from 41% to 69%, since a larger compression ratio leads to more mass transportation and enhanced deformation. The value of *w* for 800 °C accordingly increases from 1100 nm to 1490 nm, indicating the increase of the preferential growth of $Nd_2Fe_{14}B$ grains along the direction perpendicular to the pressing axis. It can be seen from Fig. 6 that the microstructure of magnets HD treated at 800 °C with 50% compression ratio consists of well aligned $Nd_2Fe_{14}B$ grains without abnormal grain growth. The sound microstructure has important influence on the magnetic properties.

3.4 Effect of hot deformation process on magnetic properties

Figure 7 shows the magnetic hysteresis loops of the SPS treated and HD treated magnets parallel and perpendicular to the pressing direction. It is observed that the hysteresis loops for the HD treated magnets have better shape and squareness than the SPS treated magnets. This means that the former has better hard magnetic properties. For the HD treated magnets, the hysteresis loops parallel to the pressing axis are quite different from those perpendicular to the pressing axis, indicating stronger anisotropy than the SPS treated magnets. This is due to the $Nd_2Fe_{14}B$ grain texture caused by the hot deformation, in which the easily magnetized axis of the magnetic grains is aligned parallel to the pressing direction [11]. The magnetic properties and degree of texture of the SPS treated and HD treated magnets parallel and perpendicular to the pressing axis are listed in Table 4. The degree of texture for the magnet HD treated at 800 °C with 69% compression ratio is 0.8115, which is much higher than 0.2051 for the SPS treated magnets. This further confirms that the HD treated magnet is strongly anisotropic. From Table 4, the deformation temperature besides deformation ratio is an important factor in hot deformation process and affects the magnetic properties of the HD treated Nd−Fe−B magnets. As shown in Figs. 8(a) and (c), the $H_{cj}^{//}$ and $(BH)_{max}^{//}$ of the HD treated magnets first increase, and then decline with the increase in deformation temperature. However, the $B_r^{//}$ keeps increasing with the deformation temperature increasing from 750 °C to 900 °C and the variation of $B_r^{//}$ is not very obvious after the deformation temperature reaches 800 °C. The maximum values of the $H_{cj}^{//}$ and $(BH)_{max}^{//}$ are obtained when the deformation temperature is 800 °C (Fig. 8(e)). The

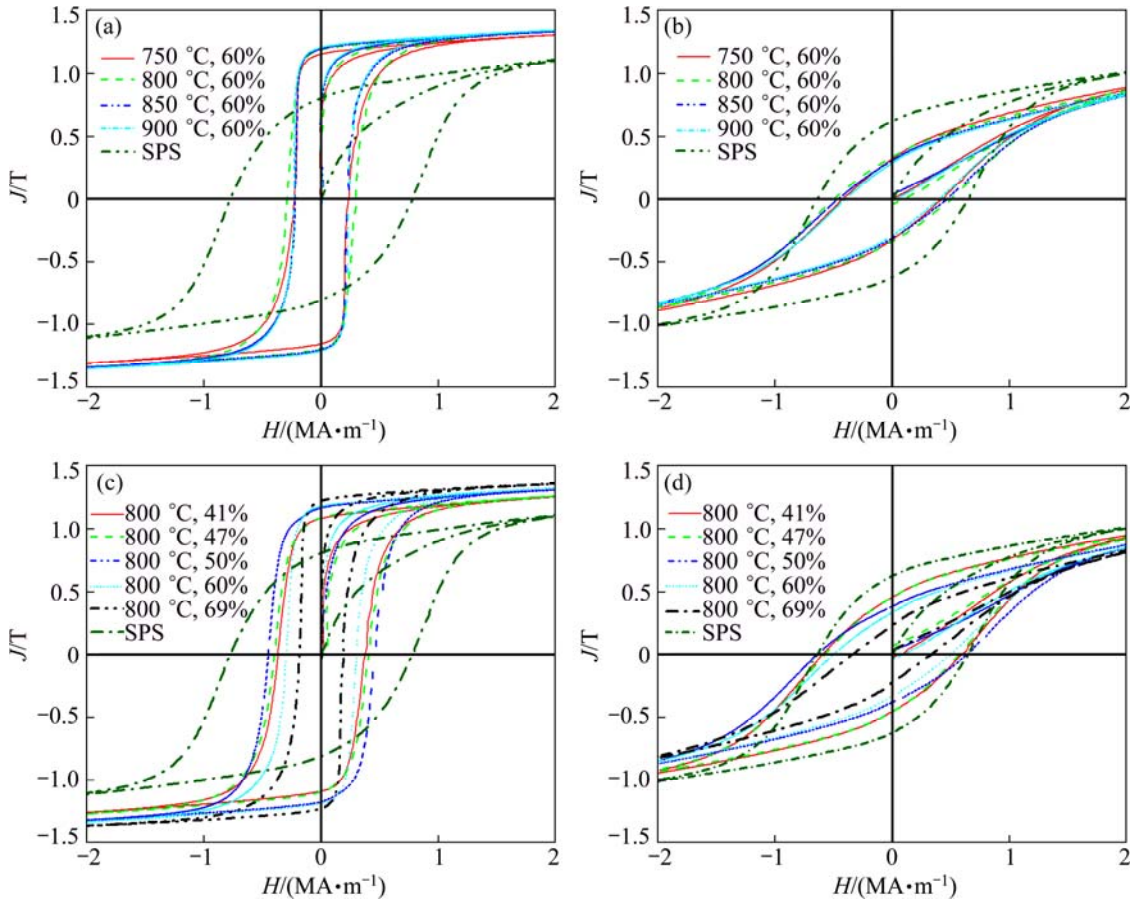

Fig. 7 Magnetic hysteresis loops of SPS treated and HD treated magnets parallel (a, c) and perpendicular (b, d) to pressing axis

remanence $B_r^{//}$ of the magnet HD treated at 800 °C is 1.19 T and less than 1.21 T at 900 °C. So, we can think that the suitable deformation temperature is 800 °C. If the deformation temperature is much higher than 800 °C, the $Nd_2Fe_{14}B$ grains will grow fast (see Fig. 6(e)), which deteriorates the coercivity. High remanence corresponding to high hot deformation temperature is strongly related to the high degree of alignment of $Nd_2Fe_{14}B$ grains.

Figures 8 (b), (d) and (f) further show the effect of compression ratio on the magnetic properties of magnets HD treated at 800 °C. With increasing the compression ratio in the range of 41%−50%, the $H_{cj}^{//}$ and $(BH)_{max}^{//}$ increase. However, the $H_{cj}^{//}$ and $(BH)_{max}^{//}$ of the HD treated magnets decline rapidly when the compression ratio increases from 50% to 69%. The increase in compression ratio results in a gradual augment in $B_r^{//}$ from 1.06 T to 1.22 T and it is consistent with the variation of microstructure shown in Fig. 6. The bulk Nd−Fe−B magnets prepared by hot deformation of HDDR powders at 800 °C with 50% compression ratio show the optimal magnetic properties along the pressing

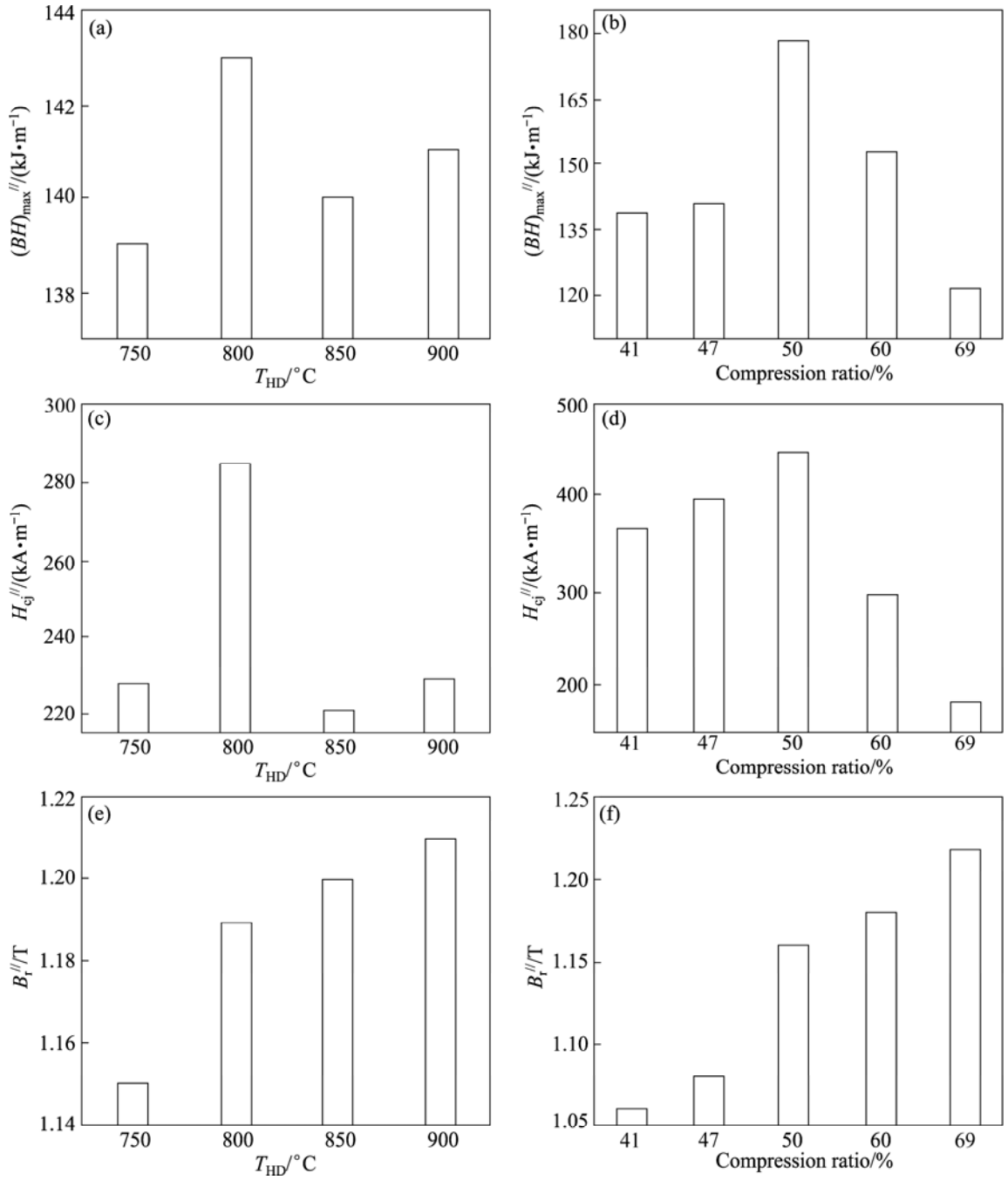

Fig. 8 Magnetic properties of hot deformed magnets as function of hot deformation temperature with 60% compression ratio (a, c, e) and as function of compression ratio at 800 °C (b, d, f)

axis: $(BH)_{max}^{//}$=178 kJ/m^3, $B_r^{//}$=1.16 T, $H_{cj}^{//}$=449 kA/m. When the compression ratio is obviously higher than 50%, the magnet is soaked at high temperatures for more time to finish the hot deformation process. As a result, abnormal grain growth will be easily induced (see Fig. 6(c)), which does harm to the coercivity.

4 Conclusions

1) For SPS treated Nd−Fe−B magnets, the B_r, H_{cj} and $(BH)_{max}$ first increase and then decrease with the increase of sintering temperature from 650 °C to 900 °C. When sintering temperature is 800 °C, the optimal magnetic properties along the sintering pressure direction were obtained: $B_r^{//}$ of 0.78 T, $H_{cj}^{//}$ of 577 kA/m and $(BH)_{max}^{//}$ of 78 kJ/m^3. The microstructure, XRD patterns and magnetic properties indicate that the magnet sintered at 800 °C is slightly anisotropic.

2) The Nd−Fe−B magnets SPS treated at 800 °C were subjected to further hot deformation at various deformation temperatures and with various compression ratios. After hot deformation, the anisotropy of magnet becomes more prominent. Compared with the starting HDDR powders or the SPS treated magnets, the HD treated magnets possess much better magnetic properties due to the strong *c*-axis texture formed in the HD process. The magnets deformed at 800 °C with 50% compression ratio parallel to the pressing axis exhibit optimal magnetic properties, such as $B_r^{//}$ of 1.16 T, $H_{cj}^{//}$ of 449 kA/m and $(BH)_{max}^{//}$ of 178 kJ/m^3.

References

[1] LI W F, OHKUBO T, HONO K, SAGAWA M. The origin of coercivity decrease in fine grained Nd−Fe−B sintered magnets [J]. Journal of Magnetism and Magnetic Materials, 2009, 321(8): 1100−1105.

[2] LIU X C, XIE R, PAN J. Magnetization arrangement of hard magnetic phases and mechanism of magnetization and reversal magnetization of nano-composite magnets [J]. Transactions of Nonferrous Metals Society of China, 2009, 19(5): 1131−1145.

[3] MISHRA R K, PANCHANATHAN V, CROAT J J. The microstructure of hot formed neodymium−iron−boron magnets with energy product 48 MGOe [J]. Journal of Applied Physics, 1993, 73(10): 6470−6472.

[4] YOSHIKAWA N, KASAI Y, WATANABE T, SHIBATA S, PANCHANATHAN V, CROAT J J. Effect of additive elements on magnetic properties and irreversible loss of hot-worked Nd−Fe−Co−B magnets [J]. Journal of Applied Physics, 1991, 69(8): 6049−6051.

[5] LIU W Q, CUI Z Z, YI X F, YUE M, JIANG Y B, ZHANG D T, ZHANG J X, LIU X B. Structure and magnetic properties of magnetically isotropic and anisotropic Nd−Fe−B permanent magnets prepared by spark plasma sintering technology [J]. Journal of Applied Physics, 2010, 107(9): 09A719.

[6] LIU X Y, WANG X, SUN H F, HU L X. MC simulation in microstructure evolution and grain growth during desorption−recombination processing of NdFeB alloy [J]. Transactions of Nonferrous Metals Society of China, 2011, 21(S2): s412−s416.

[7] LI W F, OHKUBO T, HONO K, NISHIUCHI T, HIROSAWA S. The role of grain boundaries in the coercivity of hydrogenation disproportionation desorption recombination processed Nd−Fe−B powders [J]. Journal of Applied Physics, 2009, 105(7): 07A706.

[8] TAKESHITA T, MORIMOTO K. Anisotropic Nd−Fe−B bonded magnets made from HDDR powders (invited) [J]. Journal of Applied Physics, 1996, 79(8): 5040−5044.

[9] SURESH K, OHKUBO T, TAKAHASHI Y K, OH-ISHI K, GOPALAN R, HONO K, NISHIUCHI T, NOZAWA N, HIROSAW S. Consolidation of hydrogenation-disproportionation-desorption-recombination processed Nd−Fe−B magnets by spark plasma sintering [J]. Journal of Magnetism and Magnetic Materials, 2009, 321(22): 3681−3686.

[10] LI W F, OHKUBO T, HONO K, NISHIUCHI T, HIROSAWA S. Coercivity mechanism of hydrogenation disproportionation desorption recombination processed Nd−Fe−B based magnets [J]. Applied Physics Letters, 2008, 93(5): 052505.

[11] KWON H W, KANG Y S, CHOI G S, YU J H. Effect of grain size and die-upset temperature on texture in die-upset Nd−Fe−B magnet [J]. IEEE Transactions on Magnetics, 2009, 45(6): 2590−2593.

[12] LIESERT S, KIRCHNER A, GRÜNBERGER W, HANDSTEIN A, de RANGO P, FRUCHART D, SCHULTZ L, MÜLLER K H. Preparation of anisotropic NdFeB magnets with different Nd contents by hot deformation (die-upsetting) using hot-pressed HDDR powders [J]. Journal of Alloy and Compounds, 1998, 266(1−2): 260−265.

[13] GUTFLEISCH O, KIRCHNER A, GRÜNBERGER W, HINZ D, NAGEL H, THOMPSON P, CHAPMAN J N, MÜLLER K H, SCHULTZ L, HARRIS I R. Textured NdFeB HDDR magnets produced by die-upsetting and backward extrusion [J]. Journal of Physics D: Applied Physics, 1998, 31(7): 807−811.

[14] LI Y, KIM Y B, YOON T S, SUHR D S, KIM T K, KIM C O. Coercivity enhancement by Zn addition in hot deformed NdFeB magnets [J]. Journal of Magnetism and Magnetic Materials, 2002, 242−245: 1369−1371.

[15] YUE M, TIAN M, ZHANG J X, ZHANG D T, NIU P L, YANG F. Microstructure and magnetic properties of anisotropic Nd−Fe−B magnets produced by spark plasma sintering technique [J]. Materials Science and Engineering B, 2006, 131(1−3):18−21.

[16] SONG X Y, ZHANG J X, YUE M, LI E D, ZENG H, LU N D, ZHOU M L, ZUO T Y. Technique for preparing ultrafine nanocrystalline bulk material of pure rare-earth metals [J]. Advanced Materials, 2006, 18(9): 1210−1215.

[17] LIU Z W, HUANG H Y, GAO X X, YU H Y, ZHONG X C, ZHU J, ZENG D C. Microstructure and property evolution of isotropic and anisotropic NdFeB magnets fabricated from nanocrystalline ribbons by spark plasma sintering and hot deformation [J]. Journal of Physics D: Applied Physics, 2011, 44(2): 025003

[18] SAGAWA M, FUJIMURA S, TOGAWA N, YAMAMOTO H, MATSUURA Y. New material for permanent magnets on a base of Nd and Fe (invited) [J]. Journal of Applied Physics, 1984, 55(6): 2083−2087.

[19] GRÜNBERGER W, HINZ D, KIRCHNER A, MÜLLER K H, SCHULTZ L. Hot deformation of nanocrystalline Nd−Fe−B alloys [J]. Journal of Alloy and Compounds, 1997, 257(1−2): 293−301.

[20] GUTFLEISCH O, HARRIS I R. Fundamental and practical aspects of the hydrogenation, disproportionation, desorption and recombination process [J]. Journal of Physics D: Applied Physics, 1996, 29(9): 2255−2265

[21] LEONOWICZ M, DEREWNICKA D, WOZNIAK M, DAVIES H A. Processing of high-performance anisotropic permanent magnets by die-upset forging [J]. Journal of Materials Processing Technology, 2004, 153−154: 860−867.

[22] LI L, GRAHAM C D. The origin of crystallographic texture produced during hot deformation in rapidly-quenched NdFeB permanent magnets [J]. IEEE Transactions on Magnetics, 1992, 28(5): 2130−2132.

[23] GOPLAN R, SEPEHIRI-AMIN H, SURESH K, OHKUBO T, HONO K, NISHIUCHI T, NOZAWA N, HIROSAWA S. Anisotropic Nd−Fe−B nanocrystalline magnets processed by spark plasma sintering and in situ hot pressing of hydrogenation-decomposition-desorption-recombination powder [J]. Scripta Materialia, 2009, 61(10): 978−981.

放电等离子烧结−热变形各向异性 Nd−Fe−B 磁体的微观组织及磁性能

李小强，李 力，胡 可，陈志成，屈盛官，杨 超

华南理工大学 国家金属材料近净成形工程技术研究中心，广州 510640

摘 要：采用放电等离子烧结及后续热变形技术制备各向异性 Nd−Fe−B 磁体，研究烧结温度对放电等离子烧结 Nd−Fe−B 磁体微观组织和磁性能的影响。随着烧结温度在 650~900 °C 范围内的升高，烧结态 Nd−Fe−B 磁体的剩磁、内禀矫顽力及最大磁能积呈现先升后降的趋势。在 800 °C 下烧结所获得磁体的磁性能最佳。随后，对 800 °C 烧结后具有最佳磁性能的磁体采用放电等离子烧结技术进行后续热变形处理。与初始吸氢−歧化−脱氢−再复合粉末和烧结态磁体相比，热变形磁体拥有更显著的各向异性和更好的磁性能。当热变形温度为 800 °C 且压缩比为 50%时，热变形磁体中的 $Nd_2Fe_{14}B$ 晶粒呈扁平片状且不发生异常长大；磁体沿热压方向具有最佳的磁性能：B_r、H_{cj} 和 $(BH)_{max}$ 分别为 1.16 T、449 kA/m 和 178 kJ/m^3。

关键词：Nd−Fe−B 磁体；吸氢−歧化−脱氢−再复合；放电等离子烧结；热变形；磁性能

(Edited by Xiang-qun LI)